ELSEVIER

Polymer 44 (2003) 187–197

polymer

www.elsevier.com/locate/polymer

Investigation of oxidation profile in PMR-15 polyimide using atomic force microscope (AFM)

Lili L. Johnson[a,*], R.K. Eby[a], Mary Ann B. Meador[b]

[a]*Department of Polymer Science, University of Akron, Akron, OH 44325-3909, USA*
[b]*Materials Division, NASA Glenn Research Center, Cleveland, OH 44135, USA*

Received 11 March 2002; received in revised form 23 September 2002; accepted 27 September 2002

Abstract

Nanoindentation measurements are made on thermosetting materials using cantilever deflection vs. piezoelectric scanner position behavior determined by atomic force microscope (AFM). The spring model is used to determine mechanical properties of materials. The generalized Sneddon's equation is utilized to calculate Young's moduli for thermosetting materials at ambient conditions. Our investigations show that the force-penetration depth curves during unloading in these materials can be described accurately by a power law relationship. The results show that the accuracy of the measurements can be controlled within 7%. The above method is used to study oxidation profiles in PMR-15 polyimide. The thermo-mechanical profiles of PMR-15 indicate that the elastic modulus at the surface portion of the specimen is different from that at the interior of the material. It is also shown that there are two zones within the oxidized portion of the samples. Results confirm that the surface layer and the core material have substantially different properties.

Keywords: Nanomechanical properties; PMR-15 polyimide; Atomic force microscopy

1. Introduction

The atomic force microscope (AFM) [1], also known as the scanning force microscope (SFM), is one of the most successful scanning probe microscopes (SPMs), which encompasses a family of instruments used to study surface topography and surface properties of materials on a very fine scale [2–4]. It has been an indispensable analytical tool for obtaining high-resolution images of conductive and non-conductive surfaces. The development of the AFM imaging capabilities has focused on the effects of the tip–surface interaction forces on images, leading to the utilization of the AFM as a surface force apparatus. The forces include repulsive, van der Waals, magnetic, electrostatic and capillary forces [5–9]. The ability to measure the interaction as a function of separation distance between the tip and the sample surface leads to the configuration of an AFM into a nanoindenter [10]. This allows the AFM to characterize the deformation characteristics of the materials via nanoindentation at shallow depths and low loads. The methodology of obtaining mechanical properties such as elastic modulus of materials in the literature has focused on indentation with conventional indenters in materials science and engineering [11,12]. Since AFM is a relatively new instrument, the instrumental ability to probe mechanical properties of materials needs to be evaluated and documented.

Polyimides based on the polymerization of monomeric reactants (PMR) approach are used as high temperature resistant polymer matrix materials for aircraft engine applications [13], since they combine ease of processing, high specific strength and modulus with good oxidative stability up to 316 °C. The thermo-oxidative stability (TOS) of PMR-15 polyimide has been assessed using classical methods and modern instruments [14–22]. Physical changes of PMR-15 polyimide upon aging have been examined by weight loss measurement, light optical microscopy (LM) and scanning electron microscopy (SEM). X-ray photoelectron spectroscopy (XPS), Fourier transform infrared (FTIR) spectroscopy and nuclear magnetic resonance (NMR) spectroscopy have been used to study chemical changes of PMR-15 polyimide upon aging. There is little assessment on microscopic spatial variations

* Corresponding author. Tel.: +1-330-849-5195; fax: +1-330-849-5597.
E-mail address: lljohn@aestpe.com (L.L. Johnson).

0032-3861/03/$ - see front matter © 2002 Elsevier Science Ltd. All rights reserved.
PII: S0032-3861(02)00726-7

of PMR-15 polyimide due to oxidation in the literature. Our purpose in this research is to carry out studies to: (1) develop and improve the methodology of using AFM as a nano-indentation technique; (2) utilize elastic theories to calculate the Young's modulus of polymeric materials; (3) investigate the oxidation profile in PMR-15 polyimide.

2. Experimental

2.1. Sample preparation

PMR-15 polyimide plates, (100 mm × 100 mm × 1.5 mm) were compression molded from an imidized powder commercially available from HyComp of Cleveland, OH. A 30 g charge of material was loaded into a steel tool that was then placed between the plates of a hydraulic press, which were preheated to 232 °C. Stops were used to prevent pressure on the material until the mold temperature reached 232 °C. At this point, the stops were withdrawn and contact pressure was applied and held for 10 min. After this hold, a pressure of 240 psi was applied and the temperature was ramped to 300 °C. When the die temperature reached 300 °C, the pressure was increased to 500 psi. Ramping was continued to 315 °C and the part was held under these conditions for 2 h. It was allowed to cool to below 232 °C before removal. The resulting PMR-15 polyimide plate was cut into specimens (nominally 10 mm × 10 mm × 1.5 mm) using a diamond wheel. All edge material was discarded to avoid any anomalous effects.

Nine samples were selected for isothermal aging. Three air-circulating ovens were set at the temperatures of 315, 330 and 343 °C, respectively. Three samples were placed in the middle area of each oven. The airflow rate for the ovens was set to 100 cm^3/min. The aging periods for the samples were nominally 100, 200 and 300 h.

Prior to indentation measurements using the AFM, the PMR-15 polyimide samples either un-oxidized or oxidized were mounted into epoxy to form cylinders 25 mm in diameter and 19 mm in length. The samples were mounted in a way that the cross-section of each sample is near the surface of the 25-mm diameter. These cylinders were polished to expose the cross-section of the PMR-15 polyimide materials and to achieve optical smoothness of the exposed internal sample surface. These samples were then cut by a diamond saw in a very mild lubricant into 4 mm × 4 mm × 1.5 mm pieces with the polished interior surface preserved. The small sized samples were then washed in DAWN® brand concentrated dish liquid and thoroughly rinsed in distilled water. The samples were then dried under a hood and put into a desiccator under vacuum condition for later use.

2.2. AFM as a nanoindentation technique

In this study, the sample is located on top of a tripod piezoelectric scanner that provides sample positioning in the z direction. The sample movement in the x–y plane is accomplished with a translator beneath the tripod scanner.

Force measurements are made in contact AFM by monitoring the deflection of a flexible cantilever in response to the interaction forces between the probe and the sample. Because of the sensitivity of the photodiode detector involved, the cantilever should have a spring constant (typically 10^{-2}–10^3 N/m) that is measurable. In this study, I-shaped single crystal silicon probes with the tip geometry of an asymmetrical four-sided pyramidal shape were used. The probe specification is listed in Table 1.

In the indentation experiment of AFM, the probe–sample interaction is simulated as two springs in series [23]. The Young's modulus of the materials is calculated using a generalized form of Sneddon's equation [11]

$$F = [(\xi \times E)/(1 - \upsilon^2)] \times (h - h_f)^n \quad (1)$$

where F is the applied load (nN), ξ is dependent on the contact geometry, E is the Young's modulus (Pa), υ is the Poisson's ratio, h is the current penetration depth (nm), h_f is the final depth of the contact impression after unloading (nm) and n is the tip geometry.

3. Results and discussion

3.1. Evaluation of AFM as a nanoindentation technique

The cantilever deflection-piezoelectric scanner displacement behavior of a sapphire sample was investigated first using an I-shaped silicon probe (46#6) to test the reliability of the AFM in this experiment. In Fig. 1, cantilever deflection (nA) is plotted as a function of piezoelectric scanner position (nm) for a sapphire sample. It is seen that the cantilever deflection remains unchanged before the tip–sample contact is made. After the tip contacts the sample, the cantilever deflection increases with the extension of the piezoelectric scanner in the loading process. It decreases with the retraction of the piezoelectric scanner in the unloading process and returns to its equilibrium position after the tip breaks free of the sample. It is also seen that the unloading path retraces the loading path. It indicates the linear behavior of the piezoelectric scanner and the position sensitive photodiode detector.

In Fig. 2, the cantilever deflection (nA) is plotted as a function of piezoelectric scanner position (nm) for the deflected portion of the loading curve in Fig. 1. Linear regression is used to fit the deflection data. The slope (nA/nm) is defined as the cantilever sensitivity and used to convert the deflection unit from nA to nm. Because sapphire can be considered as an infinitely hard sample compared to the stiffness of the cantilever of the silicon probe, the cantilever deflection of the probe increases or decreases linearly with the extending or retracting of the piezoelectric

Table 1
Specifications of probes used in this study

Probe ID	Cantilever/tip composition	Cantilever geometry	Cantilever length (μm)	Cantilever width (μm)	Cantilever thickness (μm)	Spring constant (N/m)	Resonant frequency (kHz)	Tip geometry	Tip radius (Å)
46#6	Silicon	I-shape	124 ± 0.2	70 ± 0.2	6.5 ± 0.2	420 ± 0.2	571 ± 0.2	Pyramidal	< 100
56#2	Silicon	I-shape	124 ± 0.2	70 ± 0.2	6.6 ± 0.2	440 ± 0.2	579 ± 0.2	Pyramidal	< 100
32#1	Silicon	I-shape	124 ± 0.2	71 ± 0.2	6.9 ± 0.2	520 ± 0.2	607 ± 0.2	Pyramidal	< 100
32#3	Silicon	I-shape	124 ± 0.2	71 ± 0.2	6.7 ± 0.2	470 ± 0.2	591 ± 0.2	Pyramidal	< 100
TM#1	Silicon	I-shape	124 ± 0.2	36 ± 0.2	4.0 ± 0.2	47.0 ± 0.2	330 ± 0.2	Pyramidal	< 100
TM#2	Silicon	I-shape	124 ± 0.2	36 ± 0.2	4.0 ± 0.2	42.0 ± 0.2	330 ± 0.2	Pyramidal	< 100

Data from Nanosensors GmbH (Germany).

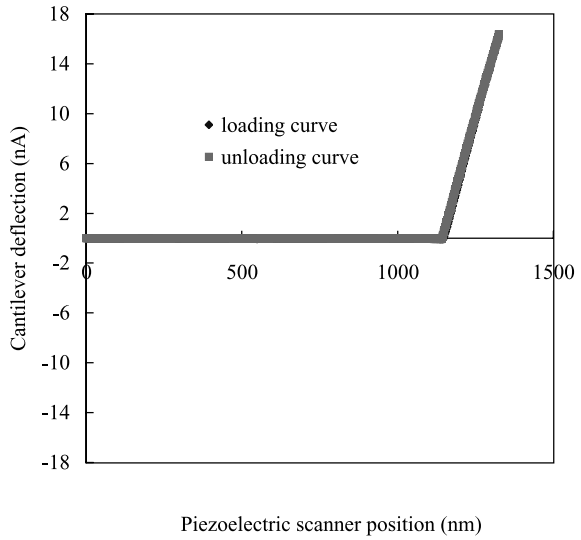

Fig. 1. Cantilever deflection (nA) vs. piezoelectric scanner position (nm) of a silicon probe (46#6) on a sapphire sample using the TopoMetrix TMX 2100.

scanner position. There is no penetration of the tip into the sapphire sample. Therefore, the linear coefficient of the data is taken as the cantilever sensitivity. Ten sets of data were collected at different locations on the sapphire sample. The average value of the cantilever sensitivity is utilized throughout this study.

The cantilever deflection as a function of piezoelectric scanner position behavior of a commercially available epoxy was investigated. This material is chosen to be a reference sample for evaluating AFM as a nanoindentation technique for thermosetting materials. There are three reasons for choosing this material as a reference sample. First, epoxy is a widely used thermosetting material and its

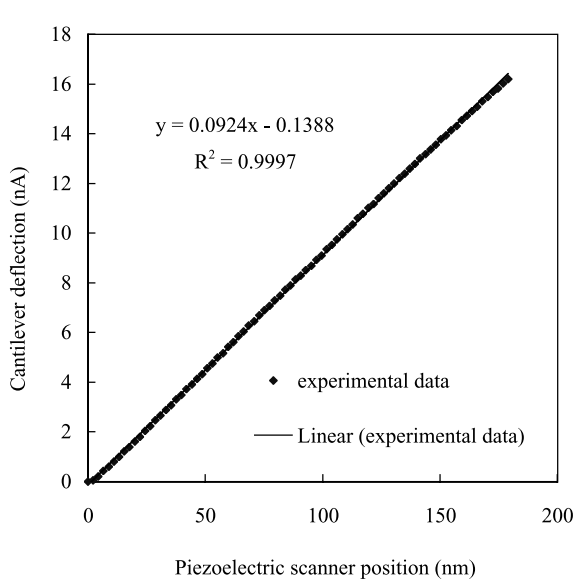

Fig. 2. Cantilever deflection (nA) vs. piezoelectric scanner position (nm) for a silicon probe (46#6) on a sapphire sample used to determine the cantilever sensitivity with the TopoMetrix TMX 2100.

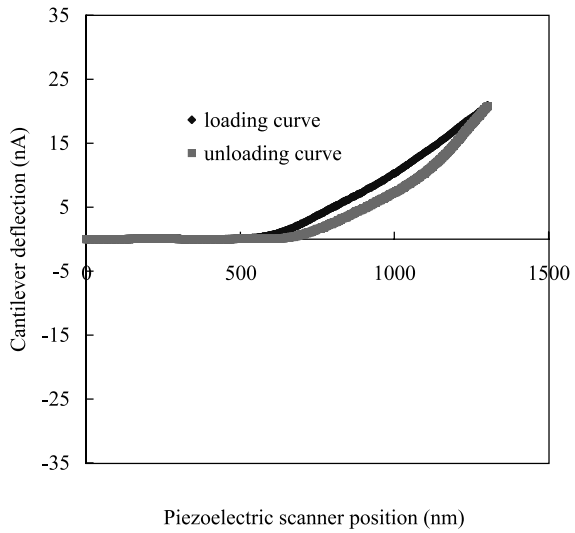

Fig. 3. Cantilever deflection (nA) vs. piezoelectric scanner position (nm) of an epoxy sample using a silicon probe (46#6) with the TopoMetrix TMX 2100.

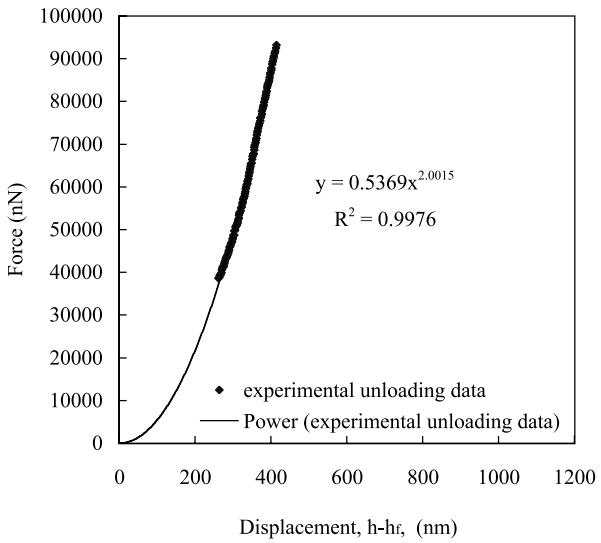

Fig. 5. Force (nN) vs. displacement between the current penetration depth and the final depth (nm) of an epoxy sample using a silicon probe (46#6) with the TopoMetrix TMX 2100.

mechanical properties can be obtained readily from the literature. Second, with the known modulus and Poisson's ratio of the epoxy, the contact geometry and tip geometry parameters of epoxy can be calculated from the generalized Sneddon's equation. Third, since PMR-15 polyimide is also a thermosetting material, the contact geometry parameters calculated for epoxy can be assumed to be the same for PMR-15 polyimide if the experimental conditions are identical. The Poisson's ratio of these two materials can also be considered to be the same. Therefore, the elastic modulus of PMR-15 polyimide can be calculated from the generalized Sneddon's equation. The cantilever deflection as a function of piezoelectric scanner position for an epoxy sample indented by a silicon probe is presented in Fig. 3. It

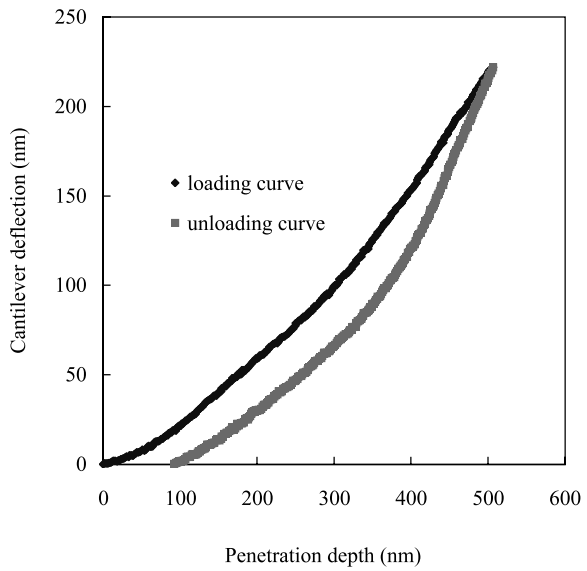

Fig. 4. Cantilever deflection (nm) vs. penetration depth (nm) of an epoxy sample using a silicon probe (46#6) with the TopoMetrix TMX 2100.

is observed that the silicon probe remains at its equilibrium condition before the tip makes contact with the sample. Starting at the contact point, the cantilever deflection increases with the extension of the piezoelectric scanner till a predetermined maximum load is reached. Then the cantilever deflection decreases with retraction of the piezoelectric scanner and returns to its equilibrium condition after the tip detaches from the sample. After tip–sample contact is made, the piezoelectric scanner position (nm) includes not only the penetration depth into the epoxy sample but also the cantilever deflection of the silicon probe. The penetration depth into the epoxy sample is calculated using the spring model and the unit of the cantilever deflection is converted using the cantilever sensitivity parameter.

The cantilever deflection (nm) as a function of penetration depth (nm) behavior of epoxy is plotted in Fig. 4. It shows that the cantilever deflection increases with increasing penetration depth in the loading process and decreases with decreasing penetration depth in the unloading process. When the load returns to zero, there is a final depth in the unloading curve. This final penetration depth is due to plastic deformation of epoxy. The plastic deformation is included in the generalized Sneddon's equation for materials in indentation experiments. Therefore, the unloading data of the epoxy sample is fitted with the generalized Sneddon's equation.

The force (nN) as a function of displacement (nm) behavior of the epoxy is shown in Fig. 5. The power law coefficient is used to calculate the contact geometry parameter (ξ) with the known values of elastic modulus and Poisson's ratio of epoxy. The power law exponent provides the tip geometry parameter (n). Ten sets of loading–unloading curves were obtained at 10 different

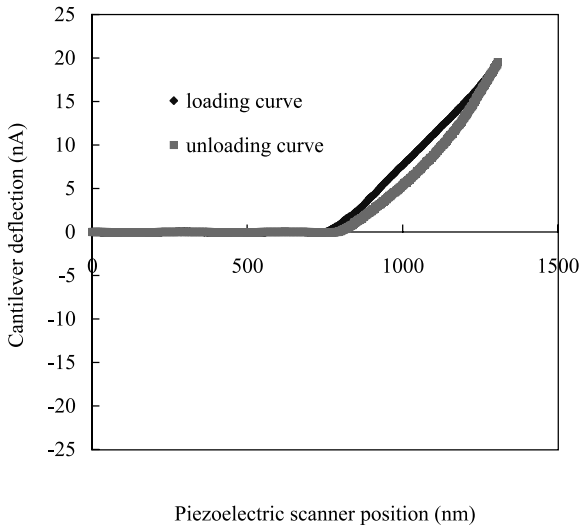

Fig. 6. Cantilever deflection (nA) vs. piezoelectric scanner position (nm) of an un-oxidized PMR-15 polyimide sample using a silicon probe (46#6) with the TopoMetrix TMX 2100.

locations on the epoxy sample. The average values of the geometry parameters for the epoxy sample are used.

The cantilever deflection (nA) vs. piezoelectric scanner position (nm) behavior of PMR-15 polyimide is investigated not only to test the reliability of the instrument but also to obtain the elastic modulus using the generalized Sneddon's equation.

Fig. 6 shows the cantilever deflection (nA) as a function of piezoelectric scanner position (nm) of an un-oxidized sample of PMR-15 polyimide. It is seen that the loading and unloading behavior of the un-oxidized PMR-15 polyimide is similar to that of the epoxy sample. The cantilever deflection (nm)–penetration depth (nm) behavior of un-

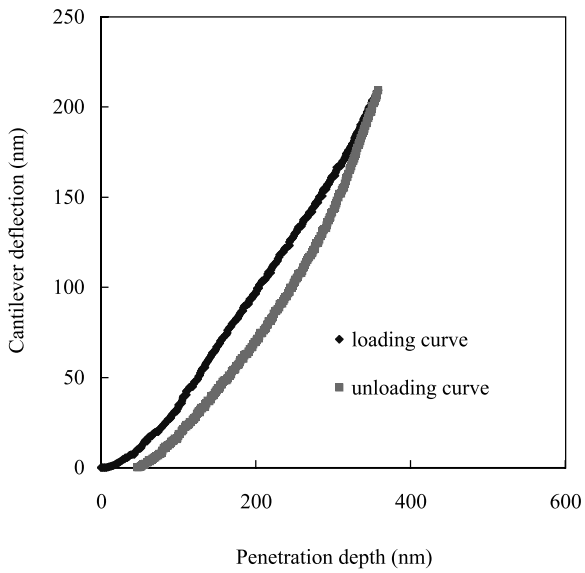

Fig. 7. Cantilever deflection (nm) vs. penetration depth (nm) for an un-oxidized PMR-15 polyimide sample using a silicon probe (46#6) with the TopoMetrix TMX 2100.

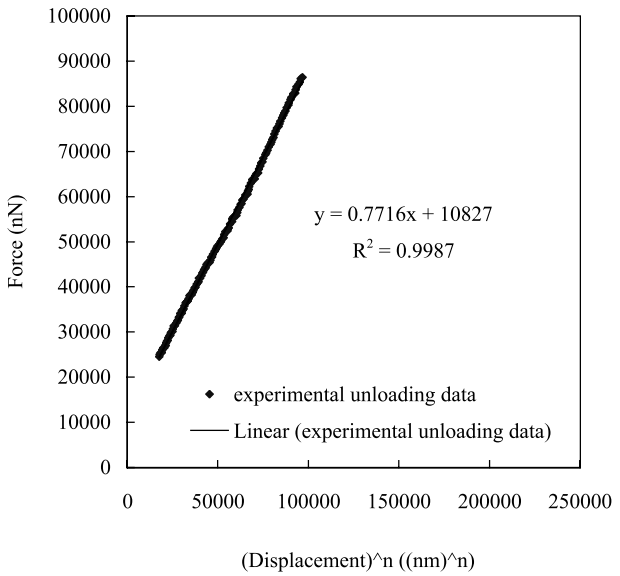

Fig. 8. Force (nN) vs. (displacement)^n ((nm)^n) of an un-oxidized PMR-15 polyimide sample using a silicon probe (46#6) with the TopoMetrix TMX 2100.

oxidized PMR-15 in Fig. 7 shows similar trends when compared with that of epoxy sample. A finite penetration depth is also observed in the unloading process. This final penetration depth is due to the plastic deformation of the un-oxidized PMR-15 polyimide in the loading process.

To calculate the elastic modulus of un-oxidized PMR-15 polyimide, the force (nN) as a function of the nth power of the displacement ((nm)^n) is plotted using the unloading data of un-oxidized PMR-15 polyimide shown in Fig. 8. It is seen that the force has a linear relationship with the nth power of the displacement. The linear coefficient contains the elastic modulus value of un-oxidized PMR-15 polyimide. By assuming the same contact geometry parameter and Poisson's ratio as that for epoxy sample, the elastic modulus of un-oxidized PMR-15 polyimide is calculated. Ten sets of loading–unloading curves of PMR-15 polyimide were performed at 10 different locations and data were processed using spring model and the generalized Sneddon's equation. The average elastic modulus measured for PMR-15 (3.31 GPa) deviates from the literature value of 3.24 Gpa [24] by about 7%.

To evaluate the repeatability of the indentation technique of AFM, another silicon probe (56#2) of the same type as 46#6 is selected. Indentation measurements were made on sapphire, epoxy and PMR-15 polyimide under the same experimental conditions. Data were collected at three different times. The average values of the contact geometry parameters (ξ and n) from epoxy and the elastic modulus (E) from PMR-15 polyimide are listed in Table 2. It is seen that consistent results are obtained at the three different dates.

The tips of these probes used in this study are in the form of a four-sided pyramid. It is necessary to evaluate the consistency of the tip geometry of these probes since

Table 2
Geometry parameters and elastic modulus obtained for testing experimental conditions using epoxy, un-oxidized PMR-15 polyimide, and a silicon probe (56#2)

Date of experiments (measurements taken at 10 different locations)									
January 5th, 2000			January 7th, 2000			January 13th, 2000			
Contact geometry (ξ)	Tip geometry (n)	Elastic modulus (E, GPa)	Contact geometry (ξ)	Tip geometry (n)	Elastic modulus (E, GPa)	Contact geometry (ξ)	Tip geometry (n)	Elastic modulus (E, GPa)
0.18	2.20	3.25	0.19	2.06	3.25	0.19	2.14	3.23
0.22	2.21	3.25	0.18	2.05	3.25	0.19	2.24	3.25
0.21	2.40	3.25	0.18	2.11	3.24	0.18	2.18	3.25
0.18	2.25	3.27	0.18	2.11	3.25	0.18	2.15	3.26
0.20	2.07	3.28	0.18	2.02	3.25	0.19	2.23	3.20
0.18	2.11	3.24	0.18	2.06	3.23	0.19	2.14	3.25
0.19	2.09	3.24	0.17	2.07	3.24	0.18	2.11	3.26
0.19	2.19	3.25	0.18	2.03	3.26	0.19	2.16	3.25
0.18	1.99	3.23	0.18	2.06	3.25	0.19	2.13	3.24
0.18	2.02	3.29	0.18	2.05	3.24	0.18	2.19	3.25
Average								
0.19	2.15	3.25	0.18	2.06	3.25	0.19	2.17	3.24

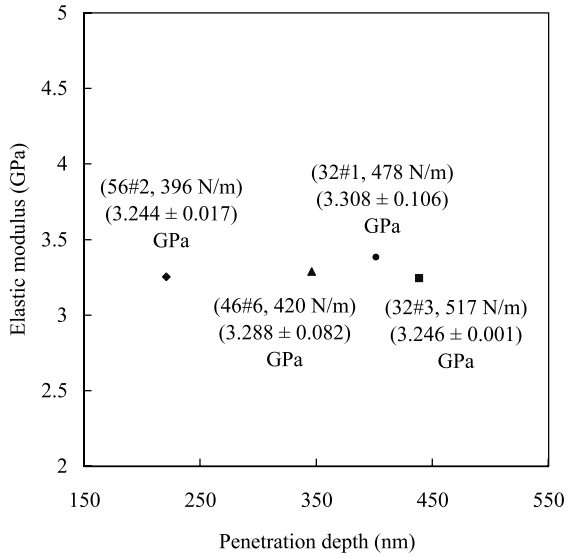

Fig. 9. The elastic modulus (Gpa) of un-oxidized PMR-15 polyimide samples determined as a function of penetration depth (nm) using four silicon probes with the TopoMetrix TMX 2100.

irregular tip geometry will cause erroneous measurements in indentation by AFM [25,26]. In order to evaluate the consistency of the geometry, four silicon probes (46#6, 56#2, 32#1 and 32#3) were used and the samples were sapphire, epoxy and un-oxidized PMR-15 polyimide. The average values of the geometry parameters obtained from epoxy samples and elastic moduli obtained from un-oxidized PMR-15 samples are listed in Table 3. This data shows that while geometry parameters vary somewhat from probe to probe, the determined values of the modulus for the PMR-15 samples are more consistent.

It has been reported that the calculated elastic modulus of materials may change with changing penetration depth due to tip defects [12,25,26]. Therefore, in this work, the elastic modulus of PMR-15 polyimide as a function of penetration depth is plotted in Fig. 9. It is seen that the elastic modulus of un-oxidized PMR-15 polyimide does not change with changing penetration depth if the geometry terms corresponding to the depth are used.

3.2. Investigation of oxidation profile in PMR-15 polyimide

Weight loss measurement has been a classical method to estimate the oxidation behavior of PMR-15 polyimide. Weight loss (%) of the PMR-15 polyimide specimens aged at 315, 330 and 343 °C as a function of aging time (h) is shown in Fig. 10. The weight loss increases with increasing aging temperature. However, the initial rate of weight loss is faster and tapers off near the end of the test especially for specimens aged at 315 and 330 °C. In Fig. 11, data are displayed on a weight-loss-rate basis. At all three temperatures, the curves are characterized by a relatively rapid initial weight loss rate that decreases as the aging time progresses and then becomes nearly constant. Similar

Table 3
The average values of geometry parameters and elastic modulus obtained for testing the consistency of tip geometry using four silicon probes, epoxy and un-oxidized PMR-15 polyimide

Probe ID	Average value of contact geometry using epoxy		Average value of tip geometry using epoxy	Average value of elastic modulus using PMR-15 polyimide (GPa)	Elastic modulus of PMR-15 polyimide from literature [25] and the percentage deviation from experimental result (GPa)
46#6	0.19		2.00	3.29	3.24 (4.62%)
56#2	0.19		2.17	3.24	3.24 (0.24%)
32#1	0.16		1.94	3.31	3.24 (6.69%)
32#3	0.57		2.00	3.25	3.24 (0.25%)

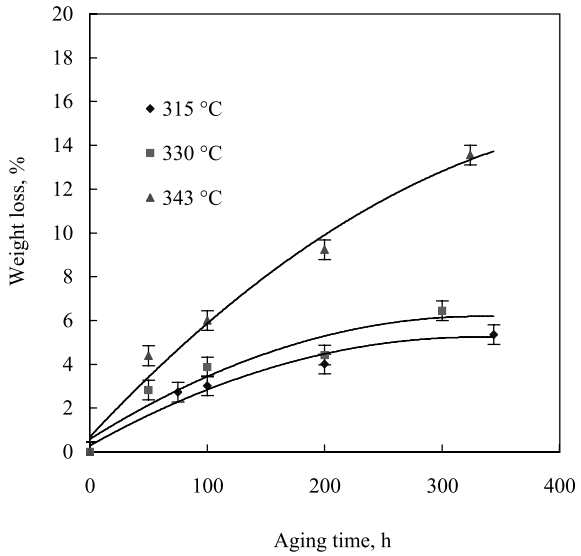

Fig. 10. PMR-15 polyimide weight loss in air at different temperatures. The error bar gives the standard deviation.

results for PMR-15 polyimide samples aged at different temperatures and time scales have been reported [14,17]. The weight loss phenomena of PMR-15 polyimide have been related to the chemical changes during oxidative attack [21].

Fig. 12 shows a cross-section of a specimen that is not aged. This sample exhibits uniformity from the sample surface to the interior of the sample, indicating there is no oxidation effect in this sample. The cross-sections shown in Figs. 13–15 of aged samples show the presence of a distinct layer that develops and grows into the polymer specimen surface due to oxidation at different aging times at elevated temperatures. Similar observations have been documented in the literature [14,17]. This layer thickens with aging time to a depth of about 100 μm and temperature and voids are

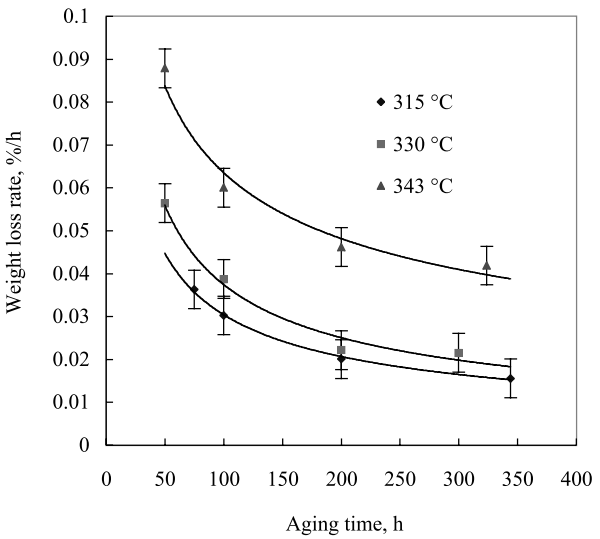

Fig. 11. PMR-15 polyimide weight loss rate in air at different temperatures. The error bar gives the standard deviation.

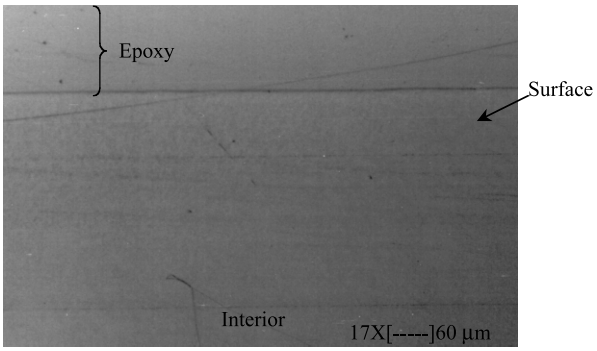

Fig. 12. Surface feature of un-oxidized PMR-15 polyimide.

observed in this layer. The size and the amount of voids increase with increasing aging time and temperature.

It has been shown by FTIR and NMR that the surface layer is chemically different from the interior of the specimen, which is the same as the initially or as cured polymer material. The formation of voids in the surface layer is related to the gaseous byproducts released during oxidation of the polymer [17,21].

Modulus (GPa) as a function of position from sample surface (µm) for PMR-15 polyimide samples aged in air at 315 °C at three different time scales is plotted in Fig. 16. The modulus profile of un-oxidized PMR-15 polyimide is also included for comparison. It is seen that the elastic modulus of the latter is about constant as the probe moves from the sample surface towards the interior of the sample. However, each of the aged samples shows up to three distinct zones on the oxidation profiles along the sample thickness.

In the region closest to the surface, the data for each sample is constant to a certain depth and the thickness increases with increasing aging time. The layer represented by this 'plateau' can be referred to as the homogeneously oxidized layer, which is the result of a zero order reaction. Beneath this reaction zone, the modulus decreases as the probing position moves towards the interior of the sample and at some point merges with that of un-oxidized PMR-15 polyimide. This reaction zone is thought to be the diffusion-controlled oxidation zone, which is the result of a first order reaction. The modulus of the inner material is unchanged by oxidation reaction. This is in agreement with microscopic

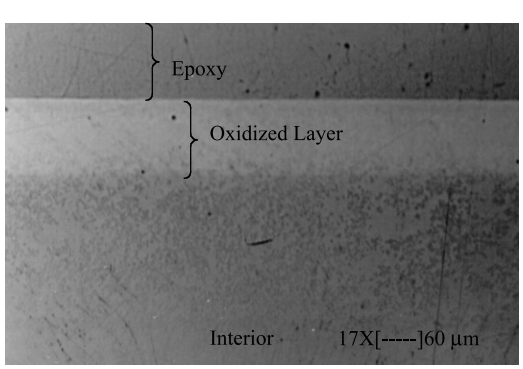

Fig. 13. PMR-15 polyimide surface degradation after aging in air at 315 °C for 344 h.

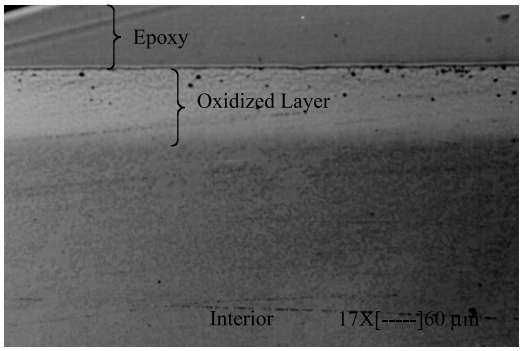

Fig. 14. PMR-15 polyimide surface degradation after aging in air at 330 °C for 300 h.

FTIR data [17], that shows that polymer in the outer layer has undergone complete oxidation but the interior is the same as an un-aged sample.

Modulus profiles of PMR-15 polyimide samples aged in air at 330 °C for three different time scales are presented in Fig. 17. These profiles show that the homogeneously oxidized layer is present for samples aged at 100 and 200 h, but not for the sample aged for 300 h. In addition, the thickness of the homogeneously oxidized layer increases with increasing aging time from 100 to 200 h.

In Fig. 18, the modulus profiles are presented for sample aged in air at 343 °C for 100, 200 and 324 h. It shows that the homogeneously oxidized layer is not observed for these three samples. Only the diffusion-controlled layer is present.

Figs. 19 and 20 show the temperature effect of the modulus profiles of PMR-15 polyimide samples aged for 100 and 200 h, respectively. It is seen that the thickness of the homogeneously oxidized layer decreases with increasing aging temperature.

The modulus profiles observed in this study are similar to profiles seen by Dole and Chauchard using pinpoint differential mechanical analysis (DMA) of heterogeneously aged poly(ethylene-*co*-methylacrylate)-based elastomer [27]. Dole and Chauchard discussed a general solution for the theoretical oxidation profile based on the rate of oxidation and the rate of the diffusion of oxygen. In their model, the oxygen concentration profile is as shown in Fig. 21. Critical oxygen concentration, $[O_2]_c$, is defined as the

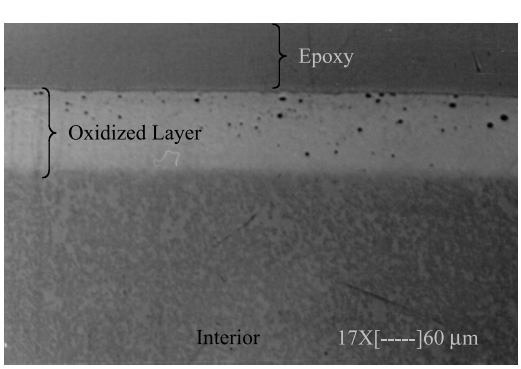

Fig. 15. PMR-15 polyimide surface degradation after aging in air at 343 °C for 324 h.

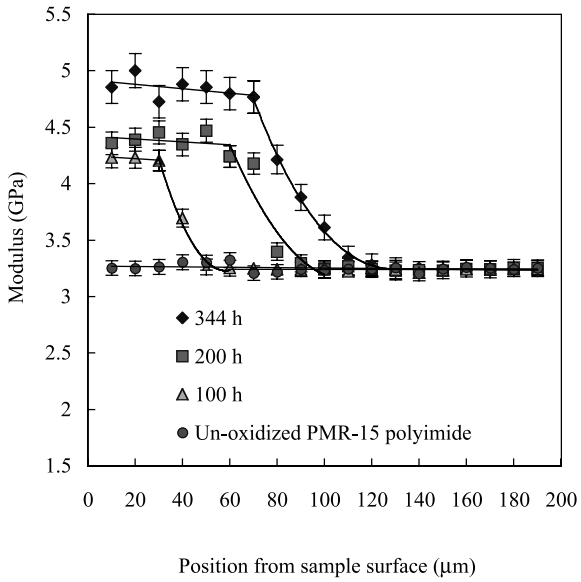

Fig. 16. Modulus profiles of PMR-15 polyimide samples aged in air at 315 °C at three different time scales and un-oxidized PMR-15 polyimide sample used as reference. The error bar gives the standard deviation.

amount necessary to oxidize the polymer at the maximum rate. Four cases can exist. In case I, the oxygen concentration at the surface is lower than $[O_2]_c$ therefore, the oxidation rate is lower than the maximum. Hence, the modulus decreases steadily from the surface to the center of the sample. For case II, the oxygen concentration at the sample surface is slightly higher than $[O_2]_c$. Again, the modulus decreases steadily from the surface to the interior, but it is higher at the surface than in case I. For case III, the oxygen concentration at the surface is much higher then $[O_2]_c$. In this case, a fraction of the sample forms a homogeneously oxidized layer where oxidation is

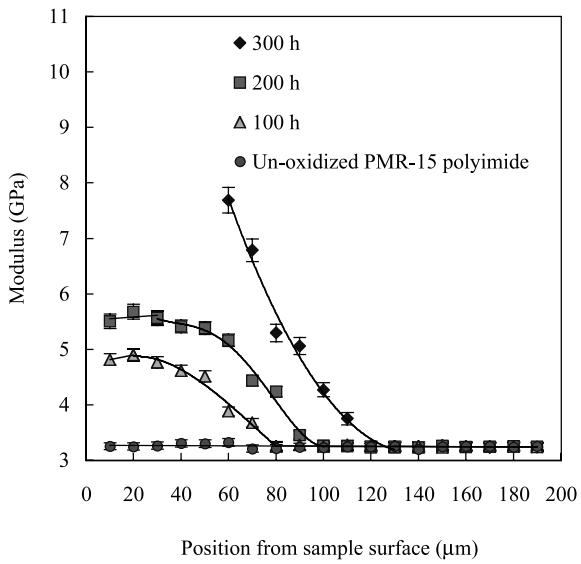

Fig. 17. Modulus profiles of PMR-15 polyimide samples aged in air at 330 °C for three different time scales and un-oxidized PMR-15 polyimide sample used as reference. The error bar gives the standard deviation.

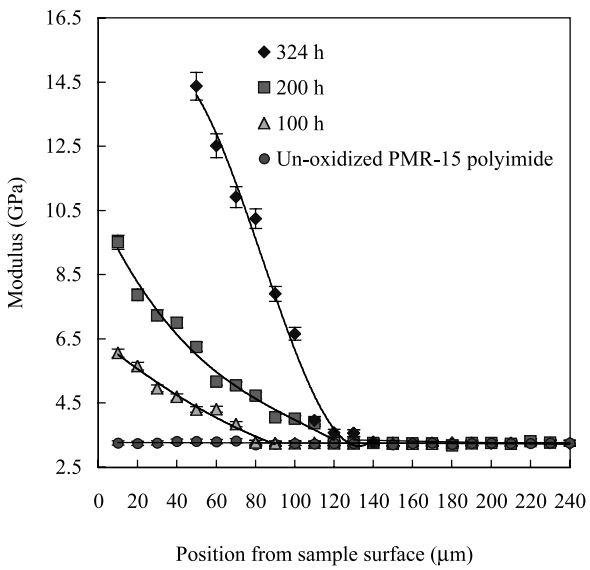

Fig. 18. Modulus profiles of PMR-15 polyimide samples aged in air at 343 °C for three different time scales and un-oxidized PMR-15 polyimide sample used as reference. The error bar gives the standard deviation.

controlled by rate of reaction rather than diffusion of oxygen. Proceeding further into the sample, is a diffusion-controlled layer as seen in cases I and II, where the oxygen concentration is again below $[O_2]_c$. Case IV is the condition in which oxygen concentration throughout the sample is above $[O_2]_c$, and therefore oxidation is homogeneous throughout the sample.

In this study, samples of PMR-15 aged at 315 °C fit case III. In each of these samples, a homogeneous oxidation layer is obtained but grows in depth with increasing aging time. At higher temperatures, the profiles fit case I or II. No homogeneous oxidation layer is produced because the maximum rate of oxidation increases with increasing

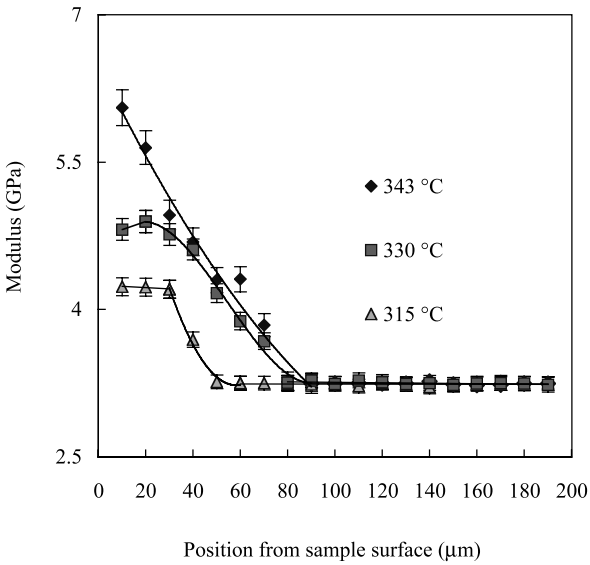

Fig. 19. Modulus profiles of PMR-15 polyimide samples aged in air at three different temperatures for 100 h.

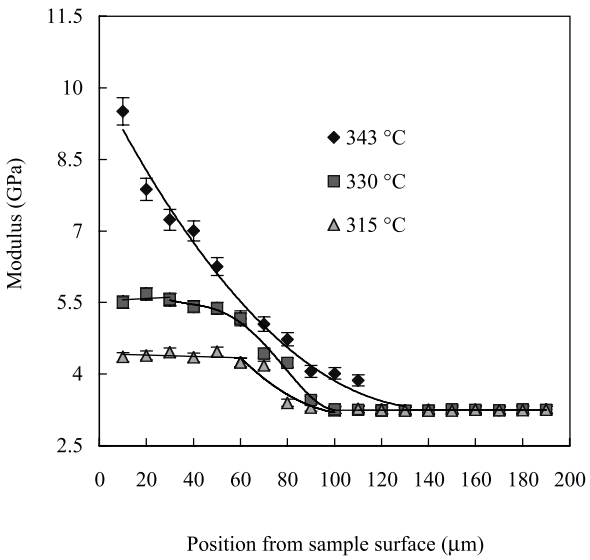

Fig. 20. Modulus profiles of PMR-15 polyimide samples aged in air at three different temperatures for 200 h.

temperature, hence the $[O_2]_c$ is never reached. These observations are consistent with studies following the chemistry of the oxidation of PMR-15 by solid ^{13}C CP-MAS NMR [21,28]. These studies follow the oxidation of the polymer labeled in specific sites with ^{13}C, and show that at 315 °C, stable products of oxidation are formed from the most vulnerable parts of the polymer (the aliphatic portions of the cross links and the polymer chain). These structures form the basis of the observed oxidation layer. Other portions of the polymer are not oxidized to any great extent at this temperature. At higher temperatures, more sites on the polymer are vulnerable to oxidation and hence, no homogenously oxidized layer is observed.

4. Conclusions

In this work, the results of carefully designed and executed experimental investigations have been reported. The experimental study consists of two parts. The first part is focused on the evaluation of AFM as a nanoindentation technique. Particular attention is given to extracting the elastic modulus of polymeric materials. The second part is focused on investigation of oxidation in PMR-15 polyimide using the AFM as a nanoindenter in which the effects of temperature and time on oxidation behavior are studied.

Results indicate that the generalized Sneddon's equation can be used to accurately describe the unloading behavior of thermosetting materials. The power law exponent is about 2, suggesting that the flat punch method of analysis for determining modulus from indentation force-penetration depth data is not entirely adequate. The contact geometry and tip geometry parameters (ξ and n) obtained using four silicon probes show fairly consistent tip shape for this type of probe. The elastic modulus determinations of the un-oxidized PMR-15 polyimide obtained using four different silicon probes indicates the parameters to be independent of penetration depth. The moduli computed by this method are within 7% of the values reported by independent means.

Detailed modulus profiles in PMR-15 polyimide samples aged at different temperatures and time scales are established confirming that AFM is capable of mapping mechanical property variations in polymers. The modulus

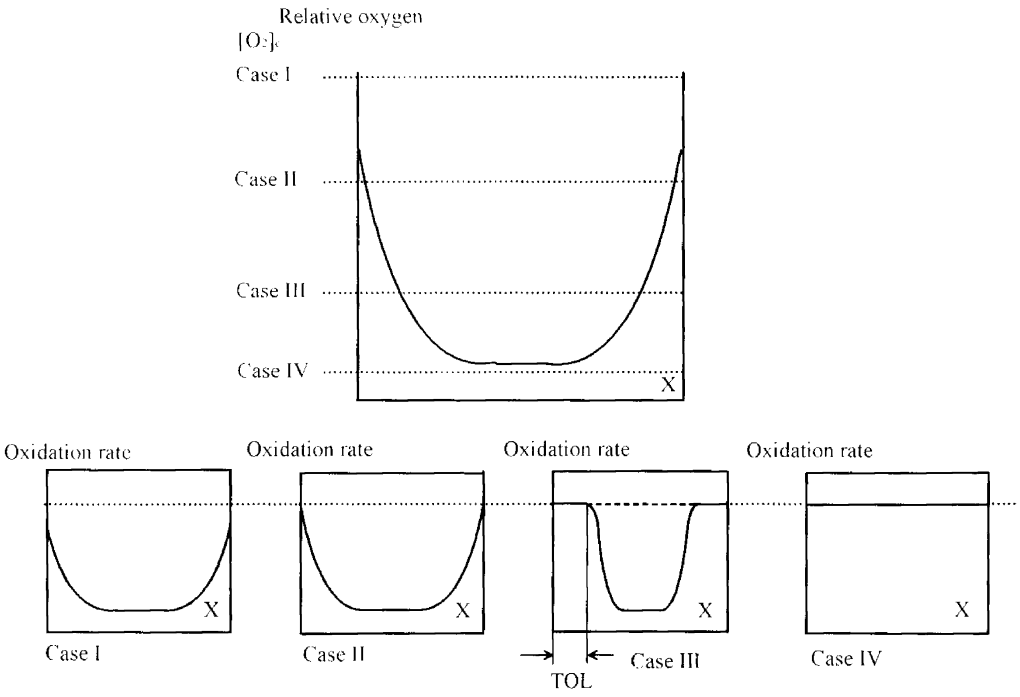

Fig. 21. Variation of the shape of the profile as a function of the critical oxygen concentration [28].

profiles in PMR-15 polyimide samples aged at 315 °C for 100, 200 and 344 h and 330 °C for 100 and 200 h show distinct zones of diffusion independent (zero order reaction) and diffusion-controlled (first order reaction) oxidation processes. The modulus profiles of PMR-15 polyimide samples aged at 343 °C indicate the absence of the diffusion independent zone and only the diffusion-controlled process.

Acknowledgements

This research was carried out by the financial support of the High Operating Temperature Propulsion Components (HOT-PC) program at NASA Glenn Research Center, which is gratefully acknowledged.

References

[1] Binnig C, Quate CF, Gerber Ch. Phys Rev Lett 1986;12:930.
[2] Marti O, Amrein M. STM and SFM in biology. London: Academic Press; 1993.
[3] Wiesendanger R. Scanning probe microscopy and spectroscopy. NY: VCH Press Syndicate of the University of Cambridge; 1994.
[4] Magonov SN, Whangbo M-H. Surface analysis with STM and AFM. Germany: VCH Verlagsgesellschatt mbH; 1996.
[5] Bruch LW. Surf Sci 1983;125:194.
[6] Bengel H, Cantow H-J, Magonov SH, Hillebrecht H, Thiele G, Liang W, Whangbo MH. Surf Sci 1995;343:95.
[7] Martin Y, Williams CC, Wickramasinghe HK. J Appl Phys 1987;61: 4723.
[8] Martin Y, Wickramasinghe HK. Appl Phys Lett 1987;50:1455.
[9] Stern JE, Terris BD, Mamin HJ, Rugar D. Appl Phys Lett 1988;53: 2717.
[10] Burnham NA, Colton RJ. J Vac Sci Technol 1989;A7:2906.
[11] Oliver WC, Pharr GM. J Mater Res 1992;7:1564.
[12] Briscoe BJ, Sebastian KS, Adams MJ. J Phys D: Appl Phys 1994;27: 1156.
[13] Meador MA, Cavano PJ, Malarik DC. Proceedings of the Sixth Annual ASM/ESD Advanced Composites Conference 1990;529.
[14] Bowles KJ, Jayne D, Leonhardt TA. SAMPE Q 1993;January:2.
[15] Alston WB, Gluyas RE, Snyder WJ, Cyclopentadiene evolution during pyrolysis–gas chromatography of PMR polyimides. NASA TN 105629, AVSCOM T. R. 91-C-023.
[16] Roberts GD, Malarik DC, Robaidek JO. Viscoelastic properties of addition-cured polyimides used in high temperature polymer matrix composites, composites design, manufacturing, and application. In: Tsai SW, Springer GS, editors. Proceedings of the Eighth International Conference on Composite Materials, vol. 12-H-1. Covina, CA: Society for Advanced Material and Process Engineering; 1991.
[17] Meador MAB, Lowell CE, Cavano PJ, Herrera-Fierro P. High Perform Polym 1996;8:363.
[18] Hay JN, Boyle JD, Parker SF, Wilson D. Polymer 1989;30:1032.
[19] Alston WB, Gluyas RE, Snyder WJ. NASA Tech Memo 1992; 105629.
[20] Simpson M, Jacobs PM, Jones FR. Composites 1991;22:105.
[21] Meador MAB, Johnston JC, Cavano PJ, Frimer AA. Macromolecules 1997;30:3215.
[22] Meador MA, Lowell CE, Johnston JC, Cavano PJ, Herrera-Fierro P. HITEMP review 1995: advanced high temperature engine materials technology program. In: Gray JR, Ginty CA, editors. NASA Conference Publication 10178, Paper 8; 1995. p. 1–12.
[23] VanLandingham MR, McKnight SH, Palsese GR, Eduljee RF, Gillespie JW, McCulough Jr. RL. J Mater Sci Lett 1997;16:117.
[24] Goodman SH. Handbook of thermoset plastics. Noyes Publications, NJ 07656; 1986. p. 310.
[25] Mareanukroh M. PhD Dissertation, University of Akron, 1999.
[26] Mareanukroh M, Eby RK, Scavuzzo RJ, Hamed GR, Preuschen J. Rubber Chem Tech 2000;73:801.
[27] Dole P, Chauchard J. Polym Degrad Stab 1995;47:411.
[28] Meador MAB, Johnston JC, Frimer AA, Gilinsky-Sharon P. Macromolecules 1999;32(17):5532–8.